Heat and Mass Transfer (2019) 55:1287–1300
https://doi.org/10.1007/s00231-018-2492-2

ORIGINAL

Experimental investigation and numerical modeling of heat transfer during solar drying of carrot slices

Archana Mahapatra [1] · P. P. Tripathy [1]

Received: 15 January 2018 / Accepted: 26 September 2018 / Published online: 3 November 2018

Abstract

The knowledge of heat transfer analysis during drying is critical for process design, quality control and energy saving. In this study, convective heat transfer coefficient, h_c during solar drying of carrot slices was determined experimentally. Carrot slices of 0.03 m diameter and 0.005 m thickness were dried in laboratory scale natural convection direct, indirect and mixed mode solar dryers. It was observed that samples dried in mixed-mode solar dryer achieved higher values of $\overline{h_c}$ (24.95 W/m^2 °C) followed by indirect (15.80 W/m^2 °C) and direct solar dryer (13.52 W/m^2 °C). Heat transfer correlations were developed during drying of carrot slices in different dryers through standard dimensionless numbers in the form of an equation $Nu = C(Ra)^n$. The results of uncertainty analysis in the $\overline{h_c}$ was observed to be in the range of 0.073%–2.7%. A numerical 2D finite element model was developed to analyse the temperature distribution inside carrot slices during drying period by using COMSOL Multiphysics simulation program. The numerical results were compared against experimental data and the outcome suggested that the sample temperatures are in close agreement with the model predictions. Lower values of statistical parameters showed better acceptability of the simulation model for predicting solar drying behaviour of carrot slices.

Abbreviations

A_p	Projected surface area of the product, m^2
A_t	Total surface area of the product, m^2
C_p	Specific heat capacity of the product, J/kg K
$e_b(T)$	Blackbody emissive power,W/m^2
G	Total incoming radiative heat flux, W/m^2
h_c	Convective heat transfer coefficient, W/m^{2}K
J	Total out-going radiative flux, W/m^2
k	Thermal conductivity of the product, W/m K
M	Moisture content, dry basis (kg water/ kg dry matter)
m_{dry}	Mass of dry matter, kg
q	Conductive heat flux, W/m^2
q_0	Inward heat flux, W/m^2
T_{air}	Average drying air temperature, K
T_{cha}	Drying chamber temperature, K
T_s	Sample temperature, K
w	Moisture content, wet basis (kg water/kg total mass)
α	Absorptivity of absorber plate
ε	Emissivity of the food product
λ	Latent heat of vaporization, kJ/kg
ρ	Density of the product, kg/m^3
σ	Stefan–Boltzmann constant, 5.67×10^{-8} W/m^2 K^4
τ	Transmissivity of glass
Φ_w	Water mass flux per second

1 Introduction

Drying is an essential method for preservation of agricultural produces for extending the shelf-life and improving quality. Major fraction of energy for industrial drying is provided by either burning fossil fuels or from electricity. However, high costs of fossil fuels, gradual depletion of its reserve and negative environmental impact have put severe constraints on their consumption [1]. On the other hand, solar energy, being one of the promising options for drying of agricultural produces at relatively low temperature, is gaining popularity nowadays. Solar dryers are broadly classified into direct, indirect [2–5] and mixed-mode [6, 7] type depending on the mode of solar heat utilization.

The drying process is governed by heat transfer from drying medium to the product and simultaneous moisture migration from the product to surrounding medium. Heat transfer to the moist product occurs mostly by convection from the surrounding air mass which is at a higher temperature than that of the product. Hence, the knowledge of convective heat transfer

✉ P. P. Tripathy
punam@agfe.iitkgp.ernet.in

[1] Agricultural and Food Engineering Department, Indian Institute of Technology, Kharagpur, West Bengal 721302, India

coefficient, h_c from drying air to the product surface is important parameter to be considered during drying process modeling. The h_c depends on drying air temperature, relative humidity, flow rate of air, exposed surface area of the product and pressure inside the drying chamber [8]. The product temperature not only influences the intermittent moisture content of the product, but also it affects the ultimate quality of the dried product. Thus, study of heat transfer coefficient is essential for accurate prediction of temperature of food product during drying in order to produce high quality, nutritious food. Several researchers in the past have determined the h_c during drying for a wide variety of food products. Anwar and Tiwari [9] have studied the h_c of green chilies, green peas, kabuli chana, onion, potato and cauliflower under forced convection drying conditions and the values were found to be 3.71, 8.22, 8.45, 14.03, 25.98 and 9.99 W/m^2 °C, respectively. Jain and Tiwari [10, 11] evaluated the h_c of cabbage and peas in open sun and in greenhouse dryer under natural and forced convection conditions. They have developed simple mathematical models to predict the crop temperature, greenhouse room temperature and moisture evaporation rate for open sun drying and greenhouse dryer. The h_c of green chilli in open sun drying and forced convection greenhouse drying were found to be 3.95 and 4.33 W/m^2 °C, respectively [12]. Tripathy et al. [13] evaluated the h_c during drying of potato cylinders in a natural convection self-tracking indirect solar dryer. They predicted that the values of h_c vary throughout the drying period ranging from 11.73–16.23 W/m^2 °C. In most of the previous literatures on heat transfer studies, a constant value of h_c is assumed for mathematical modeling. However, this assumption does not hold good as the value of h_c varies continuously during the drying process and this variation is due to the differences in drying air temperature, type of dryer, nature of food product and its physical properties like size, shape, and initial moisture content. Therefore, accurate estimation of convective heat transfer coefficient is required to fully explain the mechanism of heat transfer during the drying process.

Better understanding of the drying process is essential for improving the dryer design and for better quality products. Mathematical modeling and computer simulation makes it possible to find the optimum design and operating parameters to design a dryer as well as control strategies and analyze the effects of disturbances. Several theoretical models were used by researchers to analyze the process of heat and mass transfer during drying, which was solved using various approaches. Some of them are finite element [14, 15], finite volume [16], finite difference [17], genetic algorithm [18, 19], artificial neural network [20, 21] etc. These methods differ mainly in the assumptions made and strategies employed to solve the model equations. However, finite element method is most effective for food products with complex geometry and several studies have been reported on finite element modeling during heating and drying of food materials [22, 23]. Zhou et al. [24] studied the temperature distribution of potato slab and cylinder during microwave heating using a three dimensional finite element model. The model predicted sample temperature was in good agreement with the measured results. Heat and mass transfer during spouted bed drying of carrot cubes was modeled using Arbitrary Lagrange–Eulerian formulation and moisture content, temperature and deformation of dried particles were described successfully using the model [25]. Curcio et al. [26] considered a FE model for convective drying of carrot cylinders and their results implied that the drying performance was influenced mostly by air characteristics where the external resistance to mass transfer is the rate controlling step. Application of COMSOL Multiphysics® software for finite element modeling has been studied for various food processing operations such as mushroom blanching [27], contact baking process of pancake batter [28], coffee roasting [29], drying of prunes [30], cocoa beans [31], yacon roots [32].

The boundary conditions employed in drying process modeling are mostly influenced by h_c as the rate of heat and mass transfer are governed by this parameter. From previous studies, it was observed that determination of h_c of agricultural products considering the continuously changing drying conditions in solar dryers are limited and no reports were found for solar drying of carrots in common design of solar dryers namely, direct, indirect and mixed-mode designs. Hence, the prime objective of the present study is to evaluate the convective heat transfer coefficient of carrot slices during natural convection solar drying using direct, indirect and mixed-mode designs and to simulate the transient food temperature using finite element model during drying by considering the experimental h_c values.

2 Materials and methods

2.1 Sample selection

Fresh carrots (*Daucus carota*) were procured from the local market of Kharagpur, washed and peeled manually. Afterwards, they were cut into slices of 0.03 m diameter and 0.005 m thickness and pre-treated with hot water at 95 °C for 90 s followed by cooling in tap water and further treated with 0.5% potassium metabisulphite ($K_2S_2O_5$) solution (*w*/*v*) for 60 s with product to water ratio of 1:4 [33].

2.2 Solar drying experimentation

2.2.1 Dryer configuration

Solar drying experiments were carried out in laboratory scale natural convection direct, indirect and mixed mode

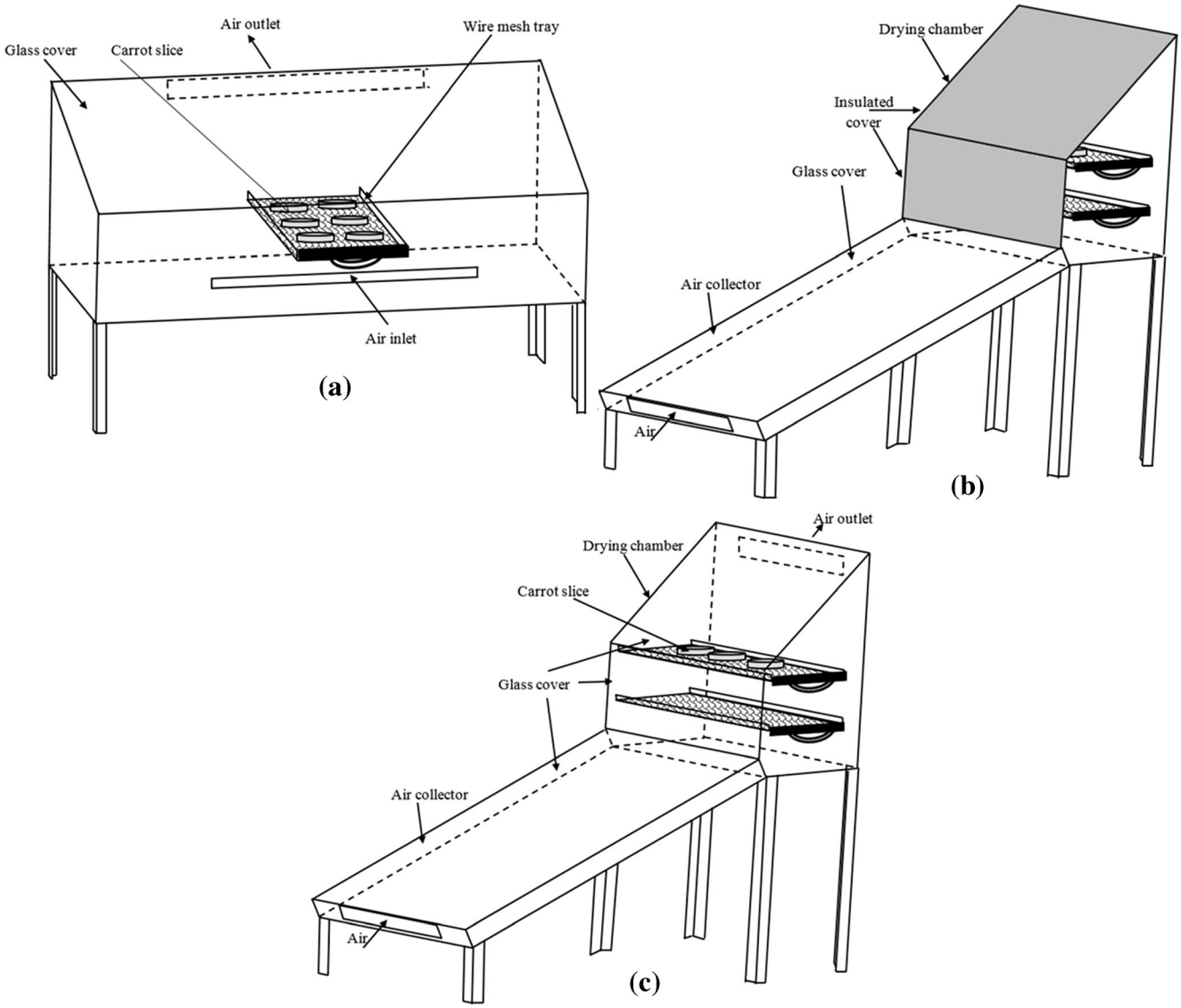

Fig. 1 Schematic diagram of (a) direct, (b) indirect and (c) mixed mode solar dryers

type solar dryers as shown in Fig. 1. In the direct or solar cabinet dryer, the food products are directly exposed to solar radiation entering through transparent top glass cover of drying chamber and no air pre heating device is provided. The solar cabinet was made of black enamel painted 22 gauge aluminium sheets and covered with 3 mm thick glass cover at the top. Rubber gaskets were provided beneath the glass cover to reduce the heat losses from the top of the dryer. The sides and bottom of the cabinet were insulated with 50 mm thick mineral wool to minimize thermal losses due to conduction. Two rectangular openings of 0.57 m × 0.01 m and 0.60 m × 0.01 m were provided at the front bottom and rear top side of the cabinet, respectively to facilitate air flow through the dryer. A wooden frame with outer aluminium foil cover was used to encase the dryer in order to protect it from adverse weather condition and was supported by mild steel angle frame.

The mixed mode and indirect solar dryers have same design from constructional point of view. Both of them have a common arrangement of pre heating the incoming air through an inclined solar collector which is connected in series to a drying chamber. The solar collector and drying chamber were made of black enamel painted 22 gauge aluminium sheets to absorb the incoming solar radiation. In case of mixed mode solar dryer, the top of the collector and drying chamber were covered with 3 mm thick glass cover to receive the solar radiation. Rubber gasket was used just beneath the glass cover to minimize top heat loss. All sides and bottom of the collector-dryer assembly were insulated by 50 mm thick mineral wool to reduce thermal loss due to conduction. Two rectangular openings of 0.34 m × 0.035 m at collector inlet and dryer outlet were provided to facilitate natural convection air flow throughout the dryer. The food products present on stainless steel wire mesh trays inside the drying chamber receives heat

from direct solar radiation as well as the preheated air coming from solar collector. The collector-dryer assembly was encased inside a wooden frame with outer aluminium foil cover to protect it from adverse weather condition and was supported by mild steel angel frame. The only difference in case of indirect solar dryer lies in the fact that food products are not directly exposed to incident solar radiation as the glass cover is replaced with an opaque cover on the top of the drying chamber. In this case, the opaque cover of 50 mm thick mineral wool insulation pad was encased in a wooden ply with outer aluminium sheet fixed on the drying chamber. All the drying experiments were carried out in clear sunshine days with the dryers positioned due south.

2.2.2 Measurement technique

Temperatures of carrot slices, drying air, drying chamber and ambient air were measured by calibrated chromel-alumel thermocouples using micro-voltmeter (accuracy ±0.01 °C). Calibrated chromel alumel thermocouples were fixed at various locations of the flat plate collector to measure the drying air temperature, inside drying chamber for assessing drying chamber temperature, inside the carrot slices to measure sample temperature and outside the dryer for ambient temperature measurement. The solar radiation intensity was measured by a calibrated pyranometer (Delta OHM, Model: LP PYRA 03, Italy). Carrot slices of about 150 g were placed on the wire mesh tray of the drying chamber for experimentation. The sample weight loss was measured at a regular interval of every 15 min for the entire drying period using a precision weighing balance (Sartorius BSA 2202S, accuracy ±0.01 g, Germany). The initial moisture content as well as the bone dry weight of samples were determined by standard oven drying method [34].

2.3 Determination of convective heat transfer coefficient

During the solar drying process, heat is transferred to the product surface by convection from hot air and by direct solar radiation from top cover of drying chamber. Assuming the temperature and moisture distribution throughout the product to be uniform initially and moisture evaporation occurring at the surface only, the sample temperature variation during drying can be described using conventional heat and mass balance equations.

The determining factor for heat transfer during solar drying process is the convective heat transfer coefficient between hot air and the product. In order to determine the accurate value of h_c during solar drying process, a methodology comprising of heat capacity of food product, solar energy absorbed by the product as well as radiative heat transfer from the drying chamber to the product has been proposed in the present study.

The resultant expression for convective heat transfer coefficient, h_c for direct and mixed-mode type solar dryer is given as:

$$m_{dry}(1+M)C_p\frac{dT_s}{dt} = h_cA_t(T_{air}-T_s) + \alpha\tau A_pG + A_t\varepsilon\sigma\left(T_{cha}^4-T_s^4\right)-\Phi_wA_t\lambda \quad (1)$$

Where, m_{dry} is the mass of dry matter, A_p and A_t are the projected and total surface area of the product. T_{air}, T_{cha} and T_s are the average drying air, drying chamber and sample temperatures, respectively. λ is the latent heat of vaporization and C_p is the specific heat capacity. ε is the emissivity of the food product, τ is the transmissivity of glass and α is the absorptivity of absorber plate. σ represents Stefan–Boltzmann constant. The thermo-physical properties of carrot were measured using empirical equations as given in Table 1.

Water mass flux per second, Φ_w in terms of moisture content, M (dry basis) is given by,

$$\Phi_w = \left(\frac{m_{dry}}{A_t}\right)\frac{dM}{dt} \quad (2)$$

Substituting Eq. (2) in (1), h_c is expressed as:

$$h_c = \frac{\left(\frac{V}{A_t}\right)\rho C_p(1+M)\left(\frac{dT_s}{dt}\right) + \frac{m_{dry}}{A_t}\left(\frac{dM}{dt}\right)\lambda - \frac{\alpha\tau A_pG}{A_t} - \varepsilon\sigma\left(T_{cha}^4-T_s^4\right)}{(T_{air}-T_s)} \quad (3)$$

In case of indirect solar dryer, due to the presence of opaque cover on the drying chamber, solar radiation does not fall directly on food products. Hence, the expression for h_c in this case can be further simplified as:

$$h_c = \frac{\left(\frac{V}{A_t}\right)\rho C_p(1+M)\left(\frac{dT_s}{dt}\right) + \frac{m_{dry}}{A_t}\left(\frac{dM}{dt}\right)\lambda - \varepsilon\sigma\left(T_{cha}^4-T_s^4\right)}{(T_{air}-T_s)} \quad (4)$$

2.4 Uncertainty analysis

During experimentation, there are several sources of errors such as instruments, calibration, measurement and testing, experimental readings etc. [8]. Solar drying of carrot slices involved measurement of temperatures of sample, hot air, ambient air, solar radiation intensity, mass of sample with various instruments. The varying accuracy of these measurement results in uncertainty calculation of h_c. Uncertainty in the experimental values is computed based on the law of propagation of uncertainty. As per recommendations of the International Organization for Standardization [35], uncertainty is taken to be equal to standard deviation. In order to determine the uncertainty during evaluation of h_c, partial derivatives were solved and values of measured variables were inserted. The

Table 1 Thermo-physical properties of carrot

Property	Equations	Unit	References
Latent heat	$\lambda = 2501.3 - 2.301T_{air} - 0.00142T_{air}^2$	kJ/kg	[38]
Bulk density	$\rho = \frac{1490(1+M)}{1+1.45M}$	kg/m^3	[39]
Specific heat	$C_p = 1.755 + 2.345w$	kJ/kg K	[40]
Thermal conductivity	$k = \frac{0.148+0.641M}{1+M}$	W/m K	[41]
Emissivity	0.95	–	[42]

details of uncertainty analysis are given in Appendix 1. Various types of errors are expressed using the following equations:

Maximum possible error in h_c,

$$E_{h_c} = \pm \sum_{i=1}^{n} \left| \frac{\partial h_c}{\partial x_i} . E_{x_i} \right| \tag{5a}$$

Statistical limit error (uncertainty) in h_c,

$$E^*_{h_c} = \pm \left[\sum_{i=1}^{n} \left(\frac{\partial h_c}{\partial x_i} \right)^2 (E_{x_i})^2 \right]^{1/2} \tag{5b}$$

where E_{xi} is the error in the measurement of x_i, representing any of the n measured variables affecting h_c.

Relative values for limit error in h_c,

$$E_{rh_c} = \pm \frac{E_{h_c}}{h_c} \tag{5c}$$

Relative values for statistical limit error in h_c,

$$E^*_{rh_c} = \pm \frac{E^*_{h_c}}{h_c} \tag{5d}$$

2.5 Formulation of finite element model

A two dimensional finite element (FE) model was developed to predict the temperature distribution during solar drying of carrot slices. The partial differential equations on heat transfer were solved using commercial software package, COMSOL Multiphysics® (Version 5.2a). Heat transfer in solids module with surface to surface radiation feature was used to illustrate heat transfer during solar drying process.

During solar drying of carrot slices, heat is mainly transferred from the surrounding hot air to the product surface by convection and from the surface to inside the product by conduction. During mixed mode and direct solar drying process, the upper surface of the product is exposed to direct solar radiation; hence an extra heat transfer interface exists in these solar dryers. As the thickness of carrot slice is very small as compared to the diameter, radial heat transfer is negligible. To simulate the process of heat transfer during solar drying of carrot slices, following assumptions were made:

a) Carrot slices are considered to be homogenous and isotropic in nature
b) Initial temperature of carrot slice is uniform throughout
c) Volume remains constant during the drying process

2.5.1 Model geometry

Carrot slice was modelled using a two dimensional axisymmetric geometry as a rectangle with axis length of 0.015 m and height of 0.005 m, representing the radius and thickness of the cylinder. Boundary 1 represents the axial symmetry, boundaries 2 and 3 represent the bottom and top surfaces and

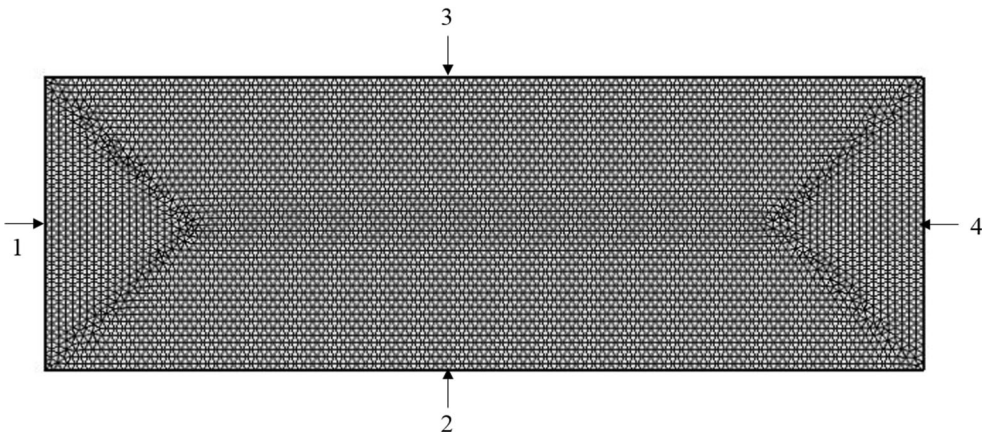

Fig. 2 Meshed geometry of a carrot slice showing different boundaries

Table 2 List of input parameters used for FE modelling of carrot

Property	Equations	Unit	References
Bulk density	$\rho = 2\times10^{-10}t^3 - 2\times10^{-6}t^2 + 0.0117t + 1071.9$(Direct) $\rho = 7\times10^{-7}t^2 - 0.0016t + 1083$ (Indirect) $\rho = 2\times10^{-6}t^2 - 0.0019t + 1080.2$(Mixed mode)	kg/m^3	[39]
Specific heat	$C_p = 6\times10^{-6}t^2 - 0.22t + 3729.3$(Direct) $C_p = 5\times10^{-6}t^2 - 0.1896t + 3726.1$ (Indirect) $C_p = 7\times10^{-6}t^2 - 0.2472t + 3763.5$(Mixed mode)	kJ/kg K	[40]
Thermal conductivity	$k = -1\times10^{-9}t^2 + 3\times10^{-6}t + 0.4354$(Direct) $k = -5\times10^{-10}t^2 - 7\times10^{-7}t + 0.44$(Indirect) $k = -1\times10^{-9}t^2 - 1\times10^{-6}t + 0.4417$(Mixed mode)	W/m K	[41]
Convective heat transfer coefficient	13.52 (Direct) 15.80 (Indirect) 24.95 (Mixed mode)	W/m^{2}K	Experimental
Radiation intensity	$G = -4\times10^{-10}t^3 + 6\times10^{-6}t^2 + 0.0022t + 636.81$ (Direct) $G = 0.0207t + 612.71$ (Mixed mode)	W/m^2	Experimental
Emissivity	0.95	–	[42]

boundary 4 represents the side surface as shown in the meshed geometry of Fig. 2. The size and shape of mesh elements are important factors in influencing convergence and accuracy of the finite element analysis [36]. The extremely fine mesh structure was selected although it led to longer computation time due to better convergence of result. An unstructured mesh with free triangular elements of size ranging between 0.15 mm to 0.3 μm was generated in COMSOL Multiphysics version 5.2a. The meshed domain contained 8470 triangular elements, 268 edge elements and 4 vertex elements.

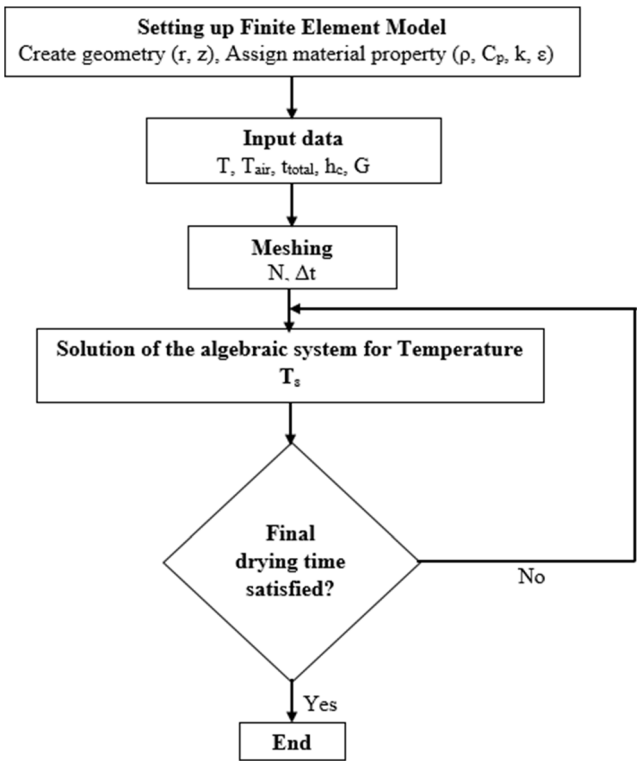

Fig. 3 Flow diagram for numerical solution of solar drying process of carrot slices

2.5.2 Governing equations

The mathematical model proposed to represent the transient heat transfer during solar drying of carrot slice is given in the form of Fourier law of heat conduction.

$$\rho C_p \frac{\partial T}{\partial t} + \nabla q = Q \tag{6}$$

$$q = -k\nabla T \tag{7}$$

Where, ρ is the density, C_p is the heat capacity, T is the temperature, q is the conductive heat flux and k is the thermal conductivity of the product.

Since heat generation inside the product is neglected, Q = 0.

The convective heat flux between drying air and product is given as:

$$-n_0.q = q_0 \tag{8}$$

$$q = h_c(T_{air} - T_s) \tag{9}$$

Heat transfer in diffuse surface is presented as:

$$-n_0.q = \varepsilon(G - e_b(T)) \tag{10}$$

$$(1-\varepsilon)G = J - \varepsilon e_b(T) \tag{11}$$

$$e_b(T) = {n_0}^2\sigma T^4 \tag{12}$$

q_0 is the inward heat flux, G is the total incoming radiative heat flux (W/m^2), $e_b(T)$ is the blackbody emissive power (W/m^2), ε is the emissivity of product, J is the total outgoing radiative flux (W/m^2) and σ is the Stefan-Boltzmann constant (W/m^{2}K^4).

2.5.3 Boundary conditions

The initial condition for heat transfer was considered to be uniform temperature throughout the sample:

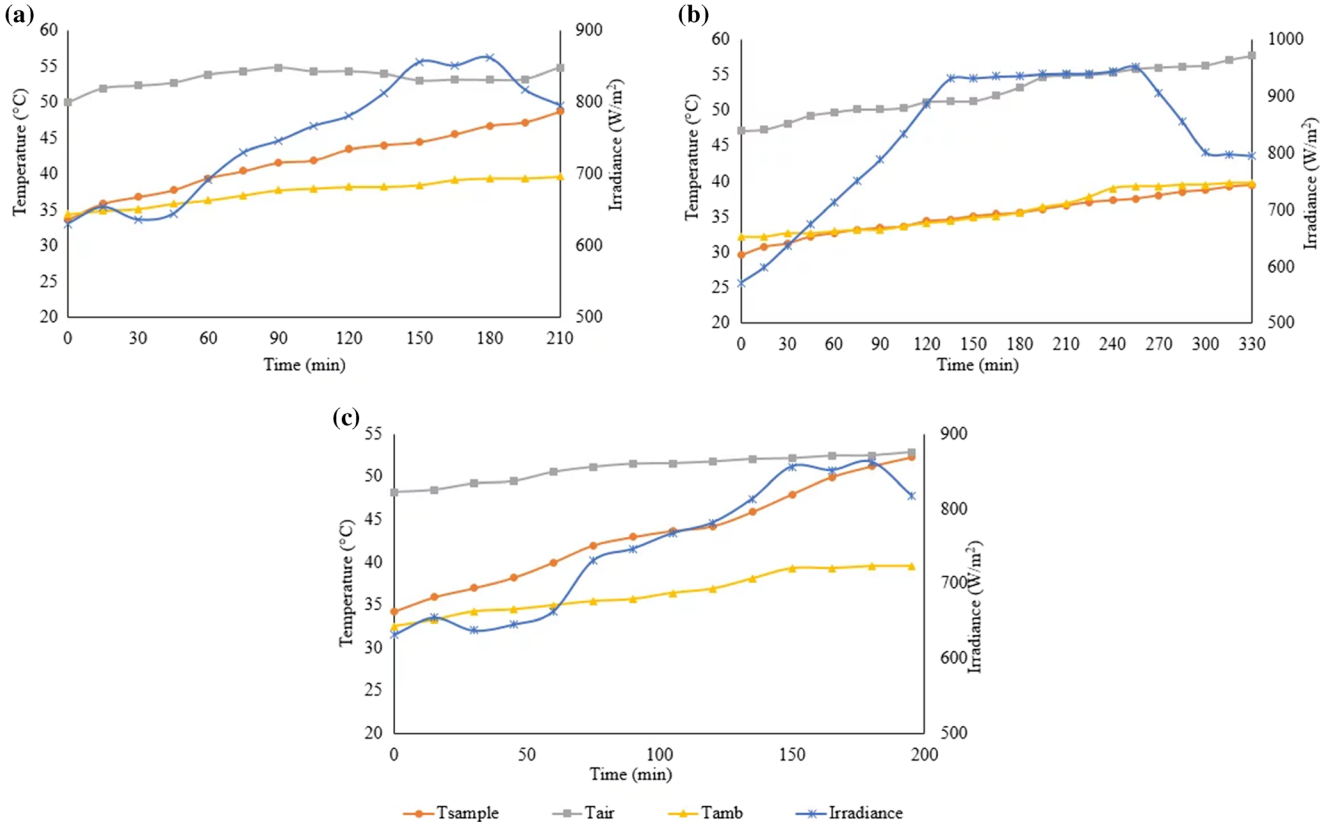

Fig. 4 Variation of product, drying air and ambient air temperature and radiation intensity during solar drying in (a) direct, (b) indirect and (c) mixed-mode solar dryer

$$T_s = T_0 \text{ at } t = t_0 \text{ for } 0 \le r \le R \text{ and } 0 \le z \le Z \tag{13}$$

Where, r and z are the space coordinates in radial and axial directions, respectively, R is the radius and Z is the thickness of carrot slices.

The boundary condition for surface 2 and 3 was convection (heat flux) in all the three drying methods, whereas an additional surface diffusion (surface to surface radiation) was considered for surface 3 in case of direct and mixed mode solar drying. Boundary condition for surface 2 and 3 in indirect solar dryer is given in Eq. (9).

Boundary condition for surface 2 and 3 of carrot slices during direct and mixed mode solar drying is given in Eqs. (9) and (14), respectively.

$$q = h_c(T_{air} - T_s) + \varepsilon(G - e_b(T)) \tag{14}$$

Boundary 4 was considered to be insulated. For insulated boundaries, the expression is given as:

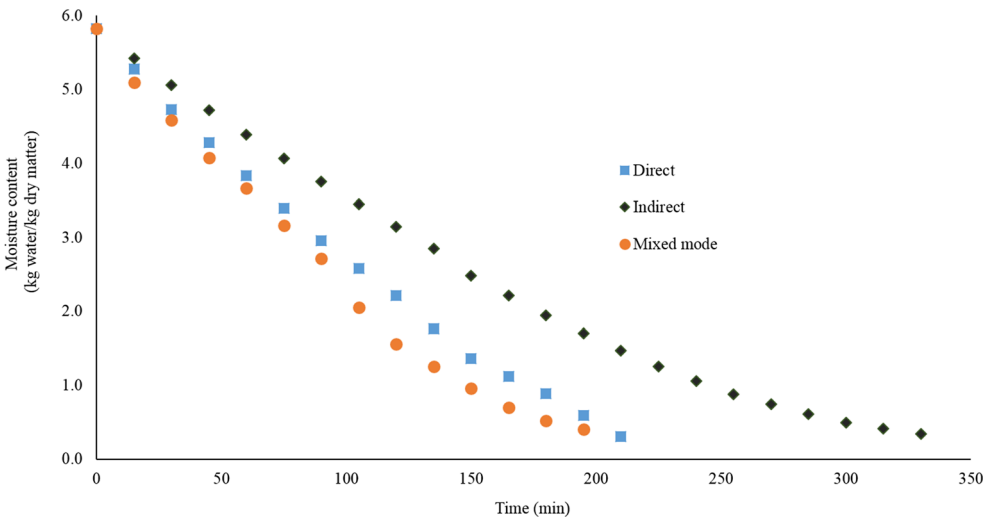

Fig. 5 Drying characteristic curve of solar dried carrot slices

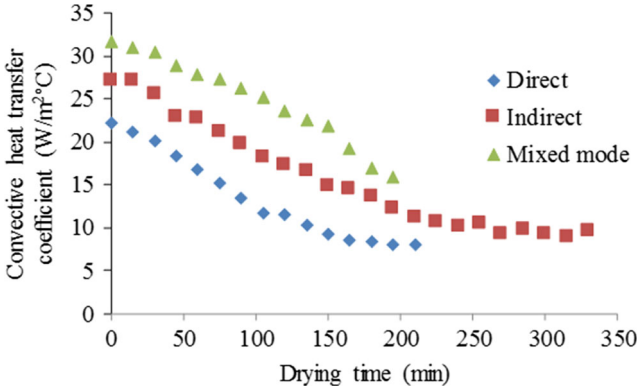

Fig. 6 Convective heat transfer coefficient of solar dried carrot slices

$$-n_0.q = 0 \tag{15}$$

The heat transfer phenomenon was conjugated by thermo-physical properties that are dependent on moisture content, temperature and time and these were obtained using empirical equations as given in Table 2. The convective heat transfer coefficient, h_c calculated from Eqs. (3) and (4) were used for numerical simulation. A time dependent study was carried out with time step of 30 s upto 12,600, 19,800 and 11,700 s, respectively for direct, indirect and mixed mode solar drying process which are the time required to reach 5% moisture content (wb) by carrot slices in the respective dryers. The model was solved according to the flow chart shown in Fig. 3.

3 Results and discussion

During solar drying of carrot slices, the moisture evaporated, temperature of sample, drying air, ambient air, drying chamber and radiation intensity were recorded at 15 min interval. The dry basis moisture content and mean sample temperature were plotted against drying time and fitted with 2nd order polynomial equations. The regression equations were further differentiated with respect to time to obtain dM/dt and dT_s/dt.

3.1 Effect of environmental conditions during drying of carrot slices

Fig 4 shows the variations of drying air temperature, food product temperature, ambient air temperature and solar radiation intensity during solar drying experimentation on carrot slices. As can be seen, the product temperature was found to vary from of 33.66–48.73 °C, 29.21–43.87 °C and 34.18–52.23 °C whereas the drying air temperature varied between 49.98–54.83 °C, 48.66–52.13 °C and 47.53–54.86 °C, respectively in direct, indirect and mixed mode solar dryers. It was seen that maximum drying air temperature was attained in mixed-mode solar dryer followed by direct and indirect dryers; as a result faster drying rate was achieved in mixed-mode solar dryer. The ambient air temperature varied between 32.2–39.7 °C during the drying period while the radiation intensity was found to be between 571 and 951 W/m^2 and maximum intensity was recorded between 10.45 AM- 2 PM.

Fig. 5 depicts the drying curve of carrot slices dried in direct, indirect and mixed-mode solar dryers. It was noticed that a drying time of 210, 330 and 195 min were taken by carrot slices to reach from an initial moisture content of 5.96, 5.83 and 5.96 kg water/ kg dry matter to a final moisture content of 0.38, 0.34 and 0.42 kg water/ kg dry matter in direct, indirect and mixed mode solar dryers, respectively. The constant rate drying period was absent in all the three cases and drying rate decreased with decreasing moisture content. The lower drying time in mixed mode solar dryer can be attributed to the fact that, the product was subjected to direct solar radiation through the glass cover in drying chamber alongside convective heat from hot air coming from the flat plate collector.

3.2 Effect of drying methods on convective heat transfer coefficient, h_c

The convective heat transfer coefficient of carrot slices during natural convection direct, indirect and mixed-mode solar drying process is shown in Fig. 6. As can be seen, h_c decreased with drying time in case of all the drying methods. The reason may be attributed to the fact that as drying proceeds, the surface evaporation stops and moisture evaporation occurs from within the product, indicating the onset of falling rate period. The h_c being a function of rate of moisture loss from the product also decreases gradually as drying proceeds. The average values of h_c during direct, indirect and mixed mode solar drying of carrot slices were found to be 13.52, 15.80 and 24.95 W/m^2 °C, respectively. It was also observed that h_c was higher in mixed-mode solar dryer followed by indirect and direct solar dryer. The presence of two drying interfaces (convective and radiative) in case of mixed-mode solar dryer leads to higher drying air temperature and faster drying. In direct solar dryer, although both drying interfaces are present, but radiation is the major mode of heat transfer and hence, h_c was found minimum for direct solar dried carrot slices.

3.3 Development of Nusselt correlation during solar drying of carrot slices

The experimental convective heat transfer coefficients obtained during direct, indirect and mixed-mode solar drying of carrot slices can be correlated using dimensionless parameters

$$Nu = \frac{h_c L_c}{k_a} = C(Gr.\mathrm{Pr})^n = C(Ra)^n \tag{16}$$

The constants C and n depend on surface geometry and flow regime respectively. Grashof number and Prandtl number can be further determined from Eqs. (17) and (18).

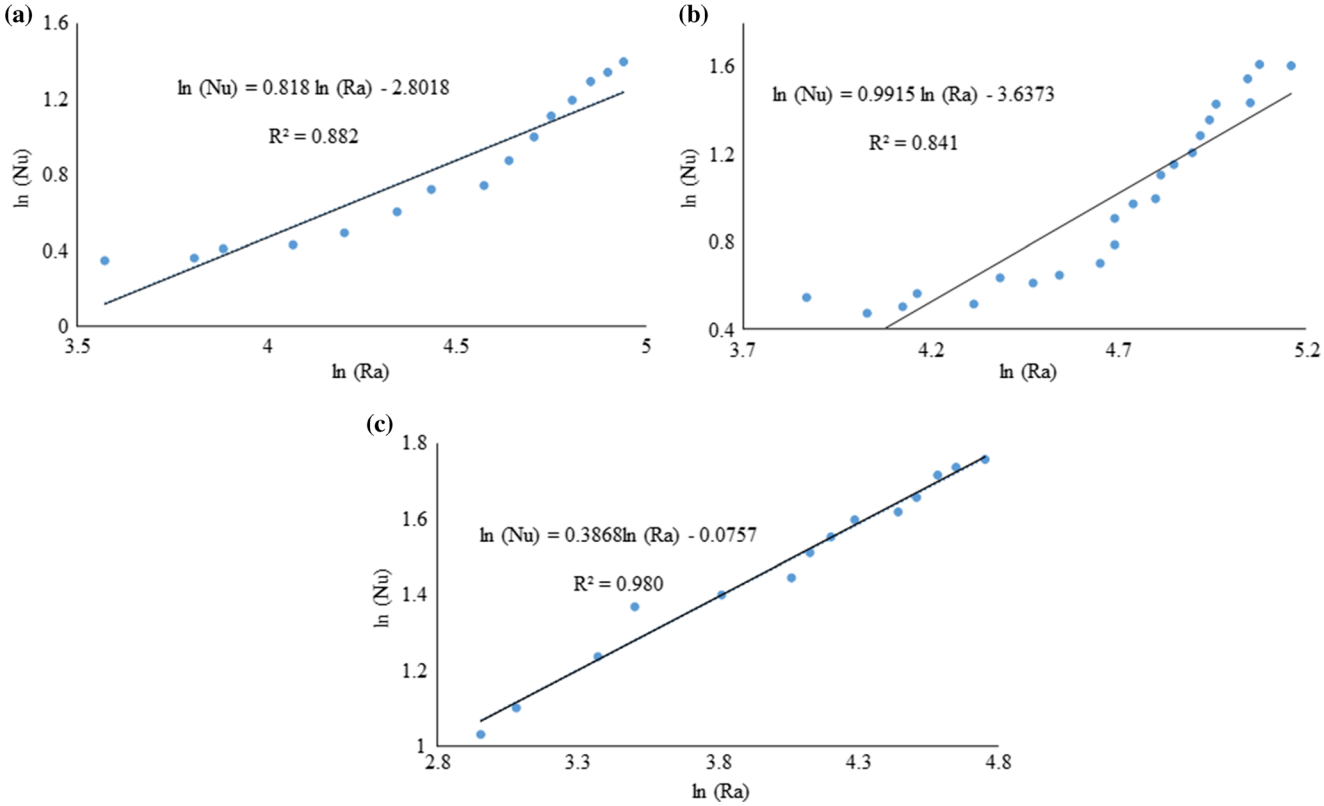

Fig. 7 Nu-Ra correlation of carrot slices dried in (a) direct, (b) indirect and (c) mixed mode solar dryer

$$Gr = \frac{g\beta\Delta T L_c^3}{\nu^2} \tag{17}$$

$$\Pr = \frac{C_p \nu \rho}{k} \tag{18}$$

where L_c is the characteristic length of the surface and is expressed as: $L_c = \frac{h}{2}$, where h is the thickness of sample, β' is the volume expansion coefficient, k is thermal conductivity, ν is viscosity of air at mean fluid temperature, $T_{fluid} = (T_{air} + T_s)/2$. These were calculated using empirical relations [37]: $\beta = 1/T_{fluid}$, $k = 0.000206T_f^{0.85}$, $\nu = 9 \times 10^{-10} T_{fluid}^{1.72}$. The value of Prandtl number was almost constant and taken as 0.7 for the temperature range of application. The experimental data of temperature and h_c were used in Eq. (16) to calculate Nusselt and Rayleigh numbers. The value of C and n were obtained from simple regression analysis.

Following correlations for Nusselt number were obtained:

$$Nu = 0.0607(Ra)^{0.818} \tag{19a}$$

$R^2 = 0.88$; Direct solar dryer

$$Nu = 0.0263(Ra)^{0.9915} \tag{19b}$$

$R^2 = 0.84$; Indirect solar dryer

$$Nu = 0.9271(Ra)^{0.3868} \tag{19c}$$

$R^2 = 0.98$; Mixed mode solar dryer

The relationship between Nusselt and Rayleigh number on semi log axes during drying of carrot slices in different solar

Table 3 Values of maximum possible error, statistical limit error, relative values of limit error and statistical limit error in experimental heat transfer coefficient during solar drying of carrot slices

Error	$\overline{h_c}$ (W/m^2°C)		
	Direct	Indirect	Mixed mode
$\overline{h_c} \pm \lvert E(h_c)\rvert$	13.52 ± 0.0113	15.80 ± 0.191	24.95 ± 0.787
$\overline{h_c} \pm \lvert E^*(h_c)\rvert$	13.52 ± 0.010	15.80 ± 0.165	24.95 ± 0.679
E_{rh_c}	±0.00084	±0.0121	±0.0315
$E^*_{rh_c}$	±0.00073	±0.0104	±0.0272

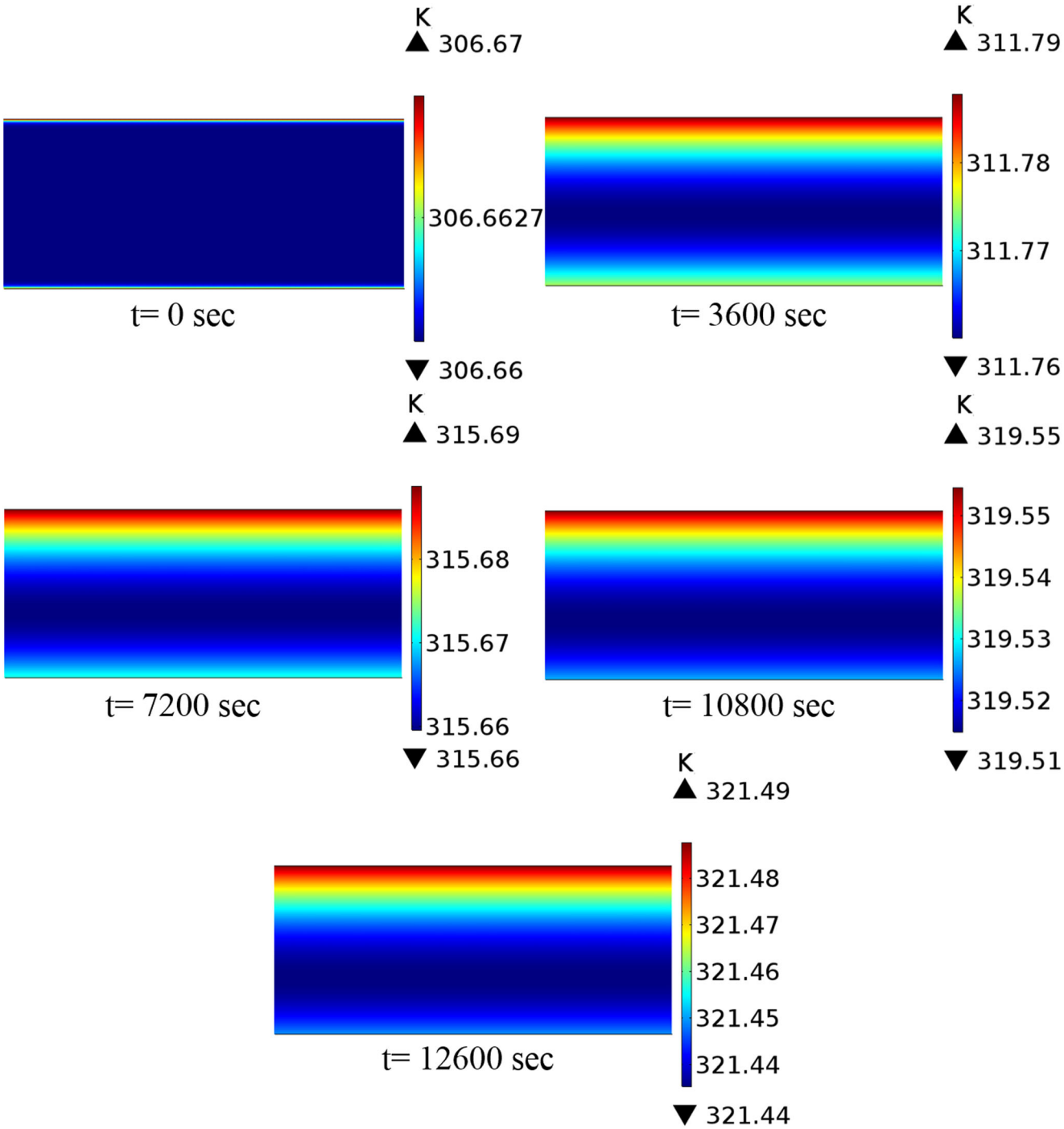

Fig. 8 Temperature distribution profile of carrot slices during direct solar drying process

dryers is illustrated in Fig. 7. Good linear correlation between ln (Nu) and ln (Ra) was observed in all the cases.

The error in experimental evaluation of $\overline{h_c}$ was estimated by uncertainty analysis and the results of error analysis are given in Table 3. *The statistical errors in* $\overline{h_c}$ *were found to be 0.073%, 1.04 and 2.7% for carrot slices dried in direct, indirect and mixed mode solar dryers, respectively.*

3.4 Computer simulation of carrot slices during solar drying process

3.4.1 Temperature distribution inside carrot slices

Figures 8, 9 and 10 show the temperature distribution inside carrot slices at every 1 h interval during direct, indirect and mixed-mode

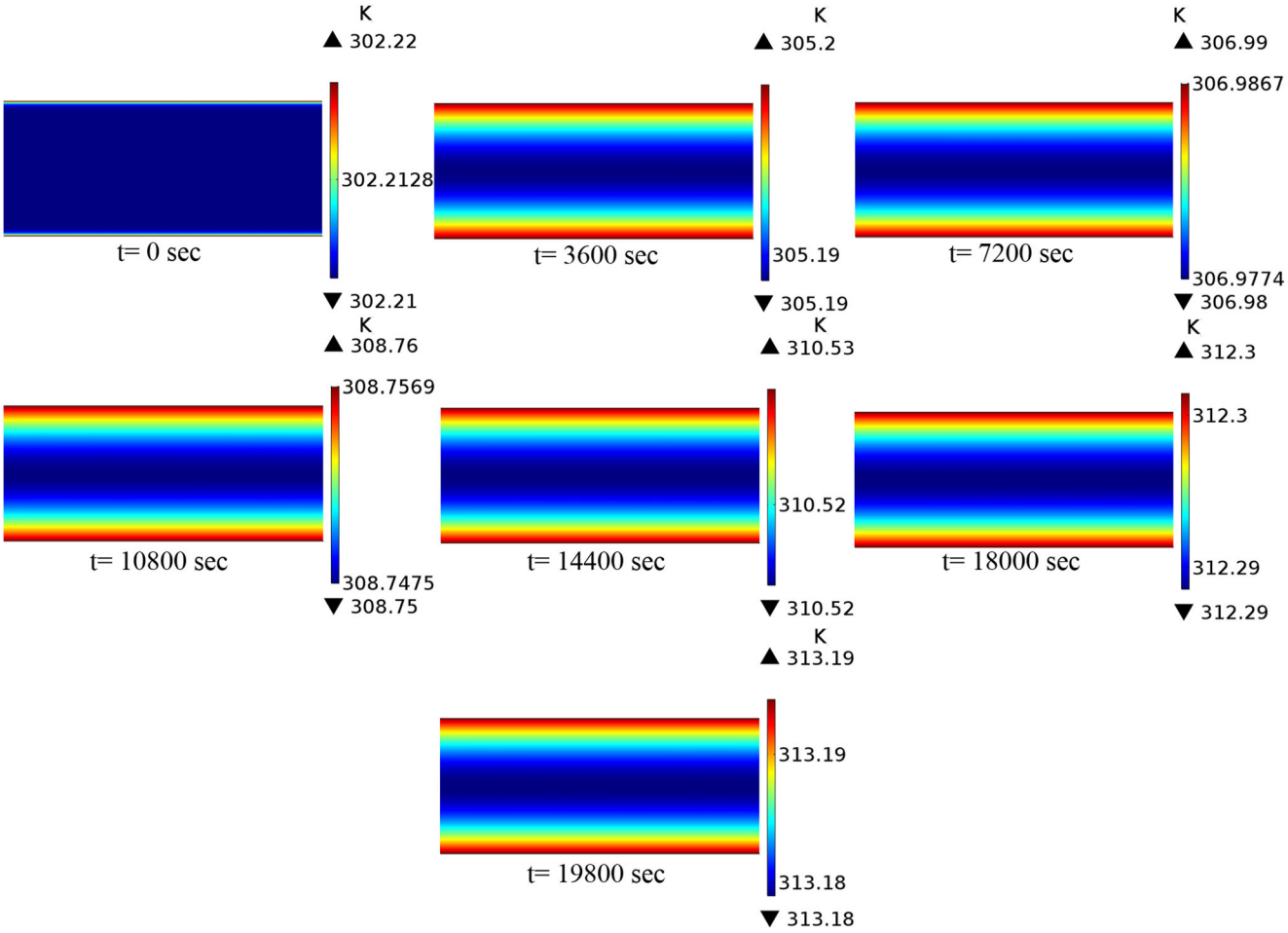

Fig. 9 Temperature distribution profile of carrot slices during indirect solar drying process

solar drying process. The colors represent temperature levels, blue being the coldest and red being the warmest; temperature range varies in each figure. At time $t = 0$, temperature of the carrot slices was uniform. The initial temperature of carrot slices was recorded to be 306.66 K, 302.21 K and 307.18 K. As drying proceeded, the temperature of air inside the drying chamber increased, thus enhancing the rate of heat transfer to the product surface. This increased the surface temperature of carrot slices and heat was conducted inside the slices. The convective heat transfer to the surface and then conductive transfer to the centre of carrot slices resulted in a temperature gradient from surface to the center of slice in all drying methods. The temperature of carrot slices increased to 321.48 K, 313.19 K and 325 K in direct, indirect and mixed mode solar dryers, respectively. In mixed mode and direct solar drying process, the top surface received additional heat due to radiation, thus further increasing the top surface temperature in these two drying methods. *The temperature difference between the hottest and coldest point of slice was found to be very less (less than 0.1 K) in each drying method*. The bottom surface temperature in direct solar dried carrot slices was less than the top surface, which indicates that radiation also plays an important role in heat transfer in addition to convection.

3.4.2 Model validation

The predictions from models were validated using statistical analysis. Fig 11 shows the experimentally obtained temperature of carrot slices and the temperature obtained from numerical simulation. As can be seen, the simulated temperature is in close agreement with the experimental temperature in all drying methods. Further, the prediction capability of the model was tested by statistical methods such as mean absolute error (MAE) and root mean square error (RMSE) in sample temperature as given below.

$$MAE = \frac{1}{N}\sum_{i=1}^{N}\left|\overline{T}_{\exp,i} - \overline{T}_{pre,i}\right| \tag{20}$$

$$RMSE = \left[\frac{1}{N}\sum_{i=1}^{N}\left(\overline{T}_{\exp,i} - \overline{T}_{pre,i}\right)^2\right]^{1/2} \tag{21}$$

Where $\overline{T}_{exp,i}$ and $\overline{T}_{pre,i}$ are the average experimental and predicted temperature of the sample for the i^{th} observation respectively and N is the number of observations. The MAE and RMSE are found to be 0.344, 0.453; 0.311, 0.368 and 0.384, 0.493 for direct, indirect and mixed mode solar dried carrot slices respectively. From

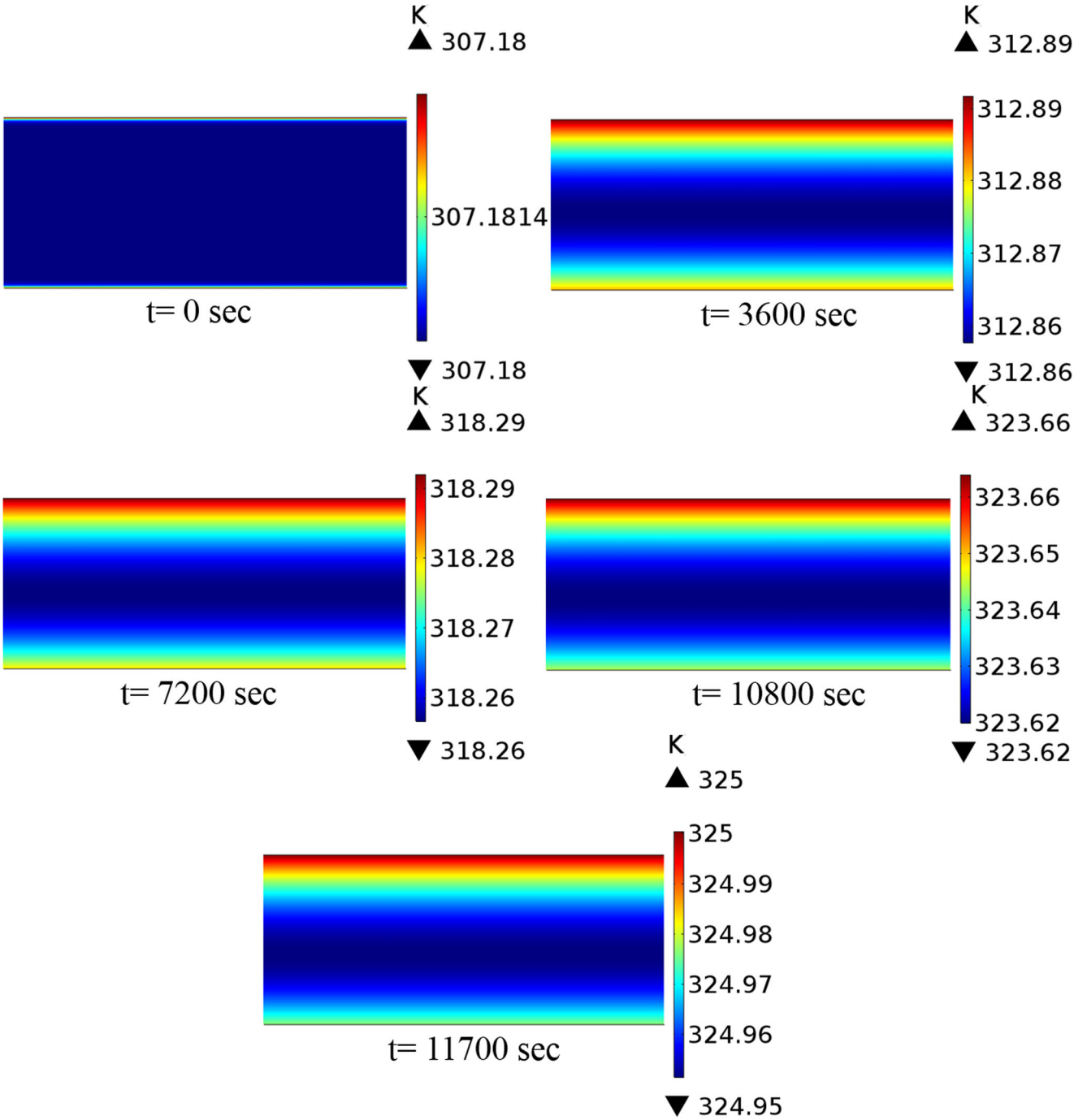

Fig. 10 Temperature distribution profile of carrot slices during mixed mode solar drying process

the lower values of statistical errors, it can be inferred that the proposed model can predict the sample temperature profile during solar drying process satisfactorily.

4 Conclusions

In the present study, convective heat transfer coefficient during solar drying of carrot slices was evaluated experimentally using laboratory scale direct, indirect and mixed mode solar dryers. The average values of h_c was found to be 13.52, 15.80 and 24.95 W/m^2 °C for direct, indirect and mixed mode solar dried carrot slices, respectively. A simplified model of heat transfer during solar drying of carrot slices was built and validated with experimental temperature data using commercial software COMSOL Multiphysics® (Version 5.2a). A good fitting between experimental and simulated temperature data was

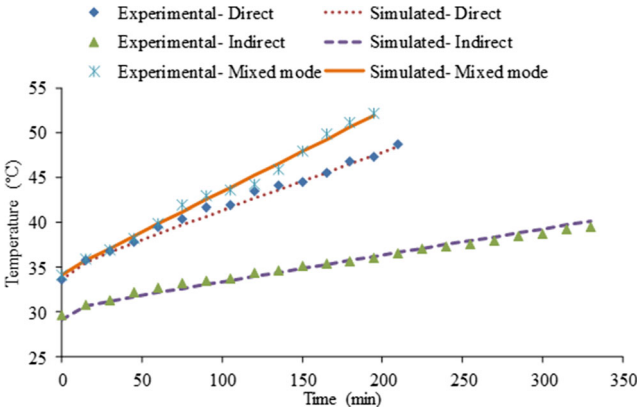

Fig. 11 Validation of temperature profile during solar drying of carrot slices

obtained from the developed model. The model can be applied to study the solar drying behaviour of different agricultural produces after appropriate implementations of the thermal-physical properties of interested materials as well as climatic conditions such as radiation intensity and ambient air temperature. Moreover, the proposed correlations of convective heat transfer coefficient and food temperature prediction model obtained for different dryer geometries would prove to be an important tool for food process engineers and solar dryer designers in specific.

Compliance with ethical standards

Conflict of interest On behalf of the co-author, the corresponding author states that there is no conflict of interest.

Appendix 1

The expression for convective heat transfer coefficient, h_c for direct and mixed mode solar dryers in Eq. (3) can be expressed as

$$h_c = \frac{(m_1-m_2)}{(t_1-t_2)}\cdot\frac{\lambda}{A_t(T_{air}-T_{s2})} + \frac{V}{A_t}\frac{\rho C_p\left(\frac{m_2}{m_{dry}}\right)}{(T_{air}-T_{s2})}\frac{(T_{s1}-T_{s2})}{(t_1-t_2)} - \frac{\alpha\tau A_p G}{A_t(T_{air}-T_{s2})} - \frac{\varepsilon\sigma\left(T_{cha}^4-T_{s2}^4\right)}{(T_{air}-T_{s2})} \quad \text{(A1.1)}$$

Similarly, the expression for h_c in Eq. (4) for indirect solar dryer can be written as

$$h_c = \frac{(m_1-m_2)}{(t_1-t_2)}\cdot\frac{\lambda}{A_t(T_{air}-T_{s2})} + \frac{V}{A_t}\frac{\rho C_p\left(\frac{m_2}{m_{dry}}\right)}{(T_{air}-T_{s2})}\frac{(T_{s1}-T_{s2})}{(t_1-t_2)} - \frac{\varepsilon\sigma\left(T_{cha}4-T_{s2}^4\right)}{(T_{air}-T_{s2})} \quad \text{(A1.2)}$$

The overall uncertainty in heat transfer coefficient of carrot slices can be calculated by partial differentiation of each variable affecting h_c in Eq. (A1.1) and (A1.2).

Overall uncertainty during direct and mixed mode solar drying of carrot slices can be expressed as

$$\left(E_{h_c}^*\right)_{overall} = \left[\left(\frac{\partial h_c}{\partial m_1}\right)^2.E^2(m_1) + \left(\frac{\partial h_c}{\partial m_2}\right)^2.E^2(m_2) + \left(\frac{\partial h_c}{\partial t_1}\right)^2.E^2(t_1) + \left(\frac{\partial h_c}{\partial t_2}\right)^2.E^2(t_2) + \left(\frac{\partial h_c}{\partial T_{s2}}\right)^2.E^2(T_{s2}) + \left(\frac{\partial h_c}{\partial T_{s1}}\right)^2.E^2(T_{s1}) + \left(\frac{\partial h_c}{\partial G}\right)^2.E^2(G) + \left(\frac{\partial h_c}{\partial R}\right)^2.E^2(R) + \left(\frac{\partial h_c}{\partial Z}\right)^2.E^2(Z)\right]^{1/2} \quad \text{(A1.3)}$$

Overall uncertainty during indirect solar drying of carrot slices can be expressed as

$$\left(E_{h_c}^*\right)_{overall} = \left[\left(\frac{\partial h_c}{\partial m_1}\right)^2.E^2(m_1) + \left(\frac{\partial h_c}{\partial m_2}\right)^2.E^2(m_2) + \left(\frac{\partial h_c}{\partial t_1}\right)^2.E^2(t_1) + \left(\frac{\partial h_c}{\partial t_2}\right)^2.E^2(t_2) + \left(\frac{\partial h_c}{\partial T_{s2}}\right)^2.E^2(T_{s2}) + \left(\frac{\partial h_c}{\partial T_{s1}}\right)^2.E^2(T_{s1}) + \left(\frac{\partial h_c}{\partial R}\right)^2.E^2(R) + \left(\frac{\partial h_c}{\partial Z}\right)^2.E^2(Z)\right]^{1/2} \quad \text{(A1.4)}$$

References

1. Fudholi A, Sopia K, Ruslan MH, Alghoul MA, Sulaiman MY (2010) Review of solar dryers for agricultural and marine products. Renew Sust Energ Rev. https://doi.org/10.1016/j.rser.2009.07.032
2. Sharma VK, Colangelo A, Spagna G (1995) Experimental investigation of different solar dryers suitable for fruit and vegetable drying. Renew Energy 6:413–424
3. Dissa AO, Bathiebo J, Kam S, Savadogo PW, Desmorieux H, Koulidiati J (2009) Modelling and experimental validation of thin layer indirect solar drying of mango slices. Renew Energy 34: 1000–1008. https://doi.org/10.1016/j.renene.2008.08.006
4. Tunde-Akintunde TY (2011) Mathematical modeling of sun and solar drying of chilli pepper. Renew Energy 36:2139–2145
5. Sallam YI, Aly MH, Nassar AF, Mohamed EA (2015) Solar drying of whole mint plant under natural and forced convection. J Adv Res 6:171–178. https://doi.org/10.1016/j.jare.2013.12.001
6. Forson FK, Nazha M a a, Akuffo FO, Rajakaruna H (2007) Design of mixed-mode natural convection solar crop dryers: application of principles and rules of thumb. Renew Energy 32:2306–2319. https://doi.org/10.1016/j.renene.2006.12.003
7. Saravanan P, Balusamy T, Srinivasan R (2015) Design, fabrication and testing of mixed mode solar dryer for vegetables. Int J Res Innov Eng Technol 1
8. Akpinar E, Midilli A, Bicer Y (2003) Single layer drying behaviour of potato slices in a convective cyclone dryer and mathematical modeling. Energy Convers Manag 44:1689–1705
9. Anwar SI, Tiwari GN (2001) Convective heat transfer coefficient of crops in forced convection drying– an experimental study. Energy

Convers Manag 42:1687–1698. https://doi.org/10.1016/S0196-8904(00)00160-6
10. Jain D, Tiwari GN (2004a) Effect of greenhouse on crop drying under natural and forced convection I: evaluation of convective mass transfer coefficient. Energy Convers Manag 45:765–783. https://doi.org/10.1016/S0196-8904(03)00178-X
11. Jain D, Tiwari GN (2004b) Effect of greenhouse on crop drying under natural and forced convection II. Thermal modeling and experimental validation. Energy Convers Manag 45:2777–2793. https://doi.org/10.1016/j.enconman.2003.12.011
12. Jain D, Mridula D, Patil RT, Barnwal P, Kumar R (2010) Kinetics of convective heat and mass transfer coefficient of green chilli during open-sun and greenhouse drying. Desalin Water Treat 24:38–46
13. Tripathy PP, Abhishek S, Bhadoria PBS (2014) Determination of convective heat transfer coefficient and specific energy consumption of potato using an ingenious self tracking solar dryer. J Food Meas Charact 8:36–45. https://doi.org/10.1007/s11694-013-9163-2
14. Ranjan R, Irudayaraj J, Reddy JN, Mujumdar AS (2004) Finite-element simulation and validation of stepwise drying of bananas. Numer Heat Transf Part A 45:997–1012
15. Pankaew P, Janjai S, Nilnont W, Phusampao C, Bala BK (2016) Moisture desorption isotherm, diffusivity and finite element simulation of drying of macadamia nut (Macadamia integrifolia). Food Bioprod Process 100:16–24
16. Oztop HF, Akpinar EK (2008) Numerical and experimental analysis of moisture transfer for convective drying of some products. Int Commun Heat Mass Transf 35:169–177. https://doi.org/10.1016/j.icheatmasstransfer.2007.06.005
17. Ramos IN, Miranda JMR, Brandão TRS, Silva CLM (2010) Estimation of water diffusivity parameters on grape dynamic drying. J Food Eng 97:519–525
18. Curvelo Santana JC, Araújo SA, Librantz AFH, Tambourgi EB (2010) Optimization of corn malt drying by use of a genetic algorithm. Dry Technol 28:1236–1244
19. Rahman MM, Mustayen AGMB, Mekhilef S, Saidur R (2015) The optimization of solar drying of grain by using a genetic algorithm. Int J Green Energy 12(12):1222–1231
20. Liu X, Chen X, Wu W, Peng G (2007) A neural network for predicting moisture content of grain drying process using genetic algorithm. Food Control 18:928–933. https://doi.org/10.1016/j.foodcont.2006.05.010
21. Khawas P, Dash KK, Das AJ, Deka SC (2016) Modeling and optimization of the process parameters in vacuum drying of culinary banana (Musa ABB) slices by application of artificial neural network and genetic algorithm. Dry Technol 34(4):491–503
22. Janjai S, Mahayothee B, Lamlert N, Bala BK, Precoppe M, Nagle M, Müller J (2010) Diffusivity, shrinkage and simulated drying of litchi fruit (Litchi Chinensis Sonn.). J Food Eng 96:214–221. https://doi.org/10.1016/j.jfoodeng.2009.07.015
23. Nilnont W, Thepa S, Janjai S, Kasayapanand N, Thamrongmas C, Bala BK (2012) Finite element simulation for coffee (Coffea arabica) drying. Food Bioprod Process 90:341–350. https://doi.org/10.1016/j.fbp.2011.06.007
24. Zhou L, Puri V, Anantheswaran R, Yeh G (1995) Finite element modeling of heat and mass transfer in food materials during microwave heating–model development and validation. J Food Eng 25:509–529
25. Białobrzewski I, Zielińska M, Mujumdar AS, Markowski M (2008) Heat and mass transfer during drying of a bed of shrinking particles - simulation for carrot cubes dried in a spout-fluidized-bed drier. Int J Heat Mass Transf 51:4704–4716. https://doi.org/10.1016/j.ijheatmasstransfer.2008.02.031
26. Curcio S, Aversa M, Calabrò V, Iorio G (2008) Simulation of food drying: FEM analysis and experimental validation. J Food Eng 87:541–553
27. Lespinard AR, Goñi SM, Salgado PR, Mascheroni RH (2009) Experimental determination and modelling of size variation, heat transfer and quality indexes during mushroom blanching. J Food Eng 92:8–17. https://doi.org/10.1016/j.jfoodeng.2008.10.025
28. Feyissa AH, Gernaey KV, Ashokkumar S, Adler-Nissen J (2011) Modelling of coupled heat and mass transfer during a contact baking process. J Food Eng 106:228–235. https://doi.org/10.1016/j.jfoodeng.2011.05.014
29. Fabbri A, Cevoli C, Romani S, Dalla Rosa M (2011) Numerical model of heat and mass transfer during roasting coffee using 3D digitised geometry. Procedia Food Sci 1:742–746. https://doi.org/10.1016/j.profoo.2011.09.112
30. Sabarez HT (2012) Computational modelling of the transport phenomena occurring during convective drying of prunes. J Food Eng 111:279–288. https://doi.org/10.1016/j.jfoodeng.2012.02.021
31. Hii CL, Law CL, Law MC (2013) Simulation of heat and mass transfer of cocoa beans under stepwise drying conditions in a heat pump dryer. Appl Therm Eng 54:264–271. https://doi.org/10.1016/j.applthermaleng.2013.02.010
32. Perussello CA, Kumar C, De Castilhos F, Karim MA (2014) Heat and mass transfer modeling of the osmo-convective drying of yacon roots (Smallanthus sonchifolius). Appl Therm Eng 63:23–32. https://doi.org/10.1016/j.applthermaleng.2013.10.020
33. Negi PS, Roy SK (2001) The effect of blanching on quality attributes of dehydrated carrots during long-term storage. Eur Food Res Technol 212:445–448. https://doi.org/10.1007/s002170000279
34. AOAC (2002) Official methods of analyses of association of analytical chemist, 15th edn. AOAC, Washington DC
35. International Organization for Standardization (1992) Guide to the expression of uncertainty in measurement, Report of International Organization for Standardization; Geneva, ISO/AG4/WG: vol. 3
36. Liu S, Fukuoka M, Sakai N (2013) A finite element model for simulating temperature distributions in rotating food during microwave heating. J Food Eng 115(1):49e62
37. Samdarshi SK, Mullick SC (1991) Analytical equation for the top heat loss factor of a flat-plate collector with double glazing. J Solar Energy Eng 113(2):117–122
38. Thorpe GR (2003) Water vapor properties. Encycl Agric food biol Eng. Marcel Dekker, Inc, New York, pp 1145–1147
39. Zogzas NP, Maroulis ZB, Marinos-Kouris D (1994) Densities, shrinkage and porosity of some vegetables during air drying. Dry Technol 12:1653–1666
40. Ratti C, Crapiste GH (1995) Determination of heat transfer coefficients during drying of foodstuffs. J Food Process Eng 18:41–53
41. Sweat VE (1974) Experimental values of thermal conductivity of selected fruits and vegetables. J Food Sci 39(6):1080–1083
42. Sinhal K, Ghoshdastidar PS, Dasgupta B (2012) Computer simulation of drying of food products with superheated steam in a rotary kiln. J Thermal Sci Eng Appl 4(1):011009